Discrete Analytical Ridgelet Transform

Philippe Carré, Eric Andres

Discrete analytical Ridgelet Transform

Philippe CARRÉ, Eric ANDRES

Laboratoire IRCOM-SIC,
bât. SP2MI, av. Marie et Pierre Curie
BP 30179 - 86960 Chasseneuil-Futuroscope Cédex - FRANCE

Abstract

In this paper, we present a new implementation of the Ridgelet transform based on discrete analytical 2-D lines: the Discrete Analytical Ridgelet Transform (DART). This transform uses the Fourier strategy (the projection-slice formula) for the computation of the associated discrete Radon transform. The innovative step of the DART is the construction of discrete analytical lines in the Fourier domain. These discrete analytical lines have a parameter called arithmetical thickness, allowing us to define a DART adapted to a specific application. Indeed, the DART representation is not orthogonal it is associated with a flexible redundancy factor (depending on the arithmetical thickness). The DART has a very simple forward/inverse algorithm that provides an exact reconstruction. We discuss the choice of the wavelet transform applied to the Radon projections and illustrate the extension of the DART to a Local-DART (with smooth windowing) and Curvelet-DART (with undecimated quincunx scheme). We apply the DART and its extensions to the denoising and the partial reconstruction of some images. These experimental results show that the simple thresholding of the DART coefficients is competitive or more effective than the classical denoising techniques.

Key words: Ridgelet Transform, Discrete Analytical Lines, Denoising, Partial Reconstruction.

1 Introduction

Image analysis is traditionally aimed at understanding digital signals obtained by sensors (in our case cameras). Digital information is considered as sampled continuous information and the theoretical background for it is signal theory. This is sometimes referred to as *"digital geometry"* in opposition to *"discrete geometry"* for computer graphics. These last ten years, since J-P. Reveillès has introduced it [16], *discrete analytical geometry* has made an important progress in defining and studying classes of discrete objects and transformations. This

greatly enhanced our understanding of the links between the discrete world $\mathbb{Z}^n$ and the continuous world $\mathbb{R}^n$. In the same time, a new discrete signal decomposition has been developed in image analysis: the wavelet representation. This new representation has many applications such as denoising, compression, analysis, etc. One of the aims of this paper is to apply this new insight in discrete geometry to image analysis and more specifically to a particular 2-D wavelet transform: the Ridgelet transform (Candès and Donoho, 1998 [5]).

Wavelets are very good at representing point singularities ; however they are significantly less efficient when it comes to linear singularities. Because edges are an extremely common phenomena in natural images, an efficient multiresolution representation of images with edges would be quite advantageous in a number of applications. A team of Stanford has recently developed an alternative system of multiresolution analysis, called Ridgelet, specifically designed to efficiently represent edges in images [5]. The Ridgelet transform can be computed by performing a wavelet analysis in the Radon domain. However, most of the work done with Ridgelets has been theorical in nature and discussed in the context of continuous functions. The important bridge to discrete implementation is tenuous at best. To our knowledge, we can find in the literature only two solutions for the discrete Ridgelet decomposition [9,18]. These two strategies are recalled in section 2. This paper presents a new approach that aims at representing linear singularities with a discrete Ridgelet transform based on discrete analytical 2-D lines: the Discrete Analytical Ridgelet Transform (DART). The idea behind the associated discrete Radon transform is to define each Radon projection by a discrete analytical line in the Fourier domain:

$$L^{\omega}_{[p,q]} = \left\{ (x_1, x_2) \in \mathbb{Z}^2 \,\middle|\, |qx_1 - px_2| \leq \frac{\omega}{2} \right\}$$

with $[p, q] \in \mathbb{Z}^2$ the direction of the Radon projection and ω, a function of (p, q), the arithmetical thickness.

There are several advantages at using discrete analytical lines: they offer a theoretical framework for the definition of the discrete Radon projections. The parameter ω allows us to define a DART adapted to specific application (control of the redundancy factor of the transform). We have used, in this paper, three types of discrete analytical lines: the closed naive lines (DART redundancy factor ≈ 2), the pythagorean lines (DART redundancy factor ≈ 2.3) and supercover lines (DART redundancy factor ≈ 3). This compares to the transform redundancies of a factor 4 for the Stanford team [18] and a factor 1 (orthogonal transform) for the Lausanne team [9].

The forward DART is based on the extraction of the 2-D Fourier coefficients belonging to the discrete analytical line $L^{\omega}_{[p,q]}$. The inverse DART is simply

performed by putting the Fourier coefficients back on the exact same place in the Fourier lattice. The DART has therefore a very simple and rapid forward/inverse algorithm. This simple straightforward approach ensures an exact reconstruction without interpolation nor iterative process (that might be sensible to noise).

In order to compare the performances of the DART, we have applied the DART and its extensions (local-DART and Curvelet-DART) to the denoising and the partial reconstruction of some images. We have compared our approach to existing ones. The recent developments have shown that the Ridgelet decomposition has very attractive results for the denoising problem [18]. For this, the Stanford team proposed to apply a thresholding on Ridgelet coefficients. Our experimental results show that the simple thresholding of the DART coefficients is competitive or more effective than the wavelet transform. Moreover the DART denoising results seems to be similar (visually and PSNR measure) than Stanford's strategy but without any iterative reconstruction algorithm and with a more flexible definition. The analysis reported here show how results of discrete analytical geometry can be successfully used in image analysis.

In section 2, we recall the continuous theory of the Ridgelet transform and describe the existing discrete Ridgelet transforms [9,18]. In section 3, we present the Discrete Analytical Radon Transform with some details on the theoretical framework of discrete analytical lines. The Discrete Analytical Ridgelet Transform (DART) is introduced at the end of the section 3. Several illustrations of the DART are proposed in the section 4. In this section, we discuss the choice of the discrete line type and 1-D wavelet transform associated with the DART. We compare also the DART with other Ridgelet transform implementations for the denoising and the partial reconstruction problematics. We present several extensions of the DART to a local-DART and to the Curvelet formalism. We end this section with some thoughts on the extension of the DART to 3-D. We conclude in section 5.

2 The Ridgelet transform

2.1 Continuous theory of Ridgelet transform

A substantial foundation for Ridgelet analysis is documented in the Ph.D. thesis of Candès [5]. The continuous Ridgelet transform of $s \in L^2(\mathbb{R}^2)$ is defined by :

$$r(a,b,\theta) = \int_{\mathbb{R}^2} \psi_{a,b,\theta}(\mathbf{x}) s(\mathbf{x}) d\mathbf{x}$$

with $\mathbf{x} = (x_1, x_2) \in \mathbb{R}^2$ and $\psi_{a,b,\theta}(\mathbf{x})$ the Ridgelet 2-D function defined from a wavelet 1-D function ψ as:

$$\psi_{a,b,\theta}(\mathbf{x}) = a^{-1/2}\psi\left(\frac{x_1\cos\theta + x_2\sin\theta - b}{a}\right)$$

$b \in \mathbb{R}$ is the translation parameter, $a \in \mathbb{R}$ is the dilatation parameter and $\theta \in [0, 2\pi[$ is the direction parameter.

The function $\psi_{a,b,\theta}$ is oriented at the angle θ and is constant along lines

$$x_1\cos\theta + x_2\sin\theta = cst$$

Transverse to these ridges it is a wavelet function. In comparison, the continuous 2-D wavelet function are tensor products of 1-D wavelets $\psi_{a,b}$ defined by:

$$\psi_{\mathbf{a},\mathbf{b}}(\mathbf{x}) = \psi_{a_1,b_1}(x_1)\psi_{a_2,b_2}(x_2) \text{ with } \psi_{a_1,b_1}(x) = a_1^{-1/2}\psi(\frac{x-b_1}{a_1})$$

With the Ridgelet transform, the translation parameters (b_1, b_2) of the 2-D wavelet transform are replaced by the line parameters (b, θ).

A basic tool for calculating Ridgelet coefficients is to view Ridgelet analysis as a wavelet analysis in the Radon domain: in 2-D, points and lines are related via the Radon transform, thus the wavelet and Ridgelet transforms are linked via the Radon transform.

The Radon transform of s is defined as:

$$Rs(\theta, t) = \int_{\mathbb{R}^2} s(\mathbf{x})\delta(x_1\cos\theta + x_2\sin\theta - t)dx_1dx_2$$

where δ is the Dirac distribution. The Ridgelet coefficients r_s of s are given by the 1-D wavelet transform to the projections of the Radon transform where the direction θ is constant and t is varying:

$$r_s(\theta, a, b) = \int_{\mathbb{R}} \psi_{a,b}(t)Rs(\theta, t)dt$$

The Radon transform can be obtained by applying the 1-D inverse Fourier transform to the 2-D Fourier transform restricted to radial lines going through the origin (this is exactly what we are going to do in the discrete Fourier domain with help of discrete analytical lines):

$$\widehat{s}(\omega\cos\theta, \omega\sin\theta) = \int_{\mathbb{R}} e^{-j\omega t}Rs(\theta, t)dt$$

with $\widehat{s}$ the 2-D Fourier transform of s.

This is the projection-slice formula that is used in image reconstruction from projection methods. All these relations are resumed in figure 1.

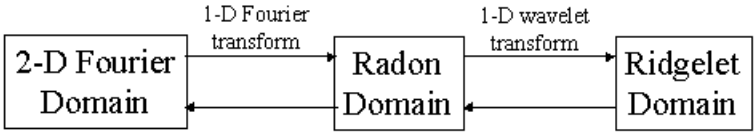

Fig. 1. Relation between transforms

2.2 Strategies for Discrete Ridgelet Transform

As we have seen, a basic strategy for calculating the continuous Ridgelet transform is first to compute the Radon transform Rs and secondly, to apply a 1-D wavelet transform to the slices $Rs(\theta, .)$. The implementation of the discrete Ridgelet transform can use the same principle.

The discrete wavelet decomposition, associated to a filter bank [15], is easy to implement, is stable and invertible, and can be associated to a discrete orthogonal representation. The discretization of the Radon transform is more difficult to achieve. The majority of methods proposed in the literature have been devised to approximate the continuous formula. None of them, however, were specifically designed to be invertible transforms for discrete images and can therefore not be used for the discrete Ridgelet transform.

The discrete Radon transform can be computed with one the two following strategies:

- Spatial strategy for digital Radon transform. The Radon transform is defined as summations of image pixels over a certain set of lines, that are defined in a finite geometry.

$$Rs([p,q],b) = \sum_{(x_1,x_2)\in L_{[p,q],b}} s(x_1,x_2)$$

  with $L_{[p,q],b} = \{(x_1,x_2) \in [0,N-1] \times [0,N-1] : qx_1 - px_2 - b = 0\}$ and (p,q) the normal vector.
- Fourier strategy for digital Radon transform. The projection-slice formula suggests that approximate Radon transforms for digital data can be based on discrete Fast Fourier transforms (FFT). The Fourier-domain computation of an approximate digital Radon transform is defined as:

(1) Compute the 2-D FFT of s

(2) Extract Fourier coefficients along the lines L_θ going through the origin.
(3) Compute the 1-D inverse FFT on each line L_θ (defined for each value of the angular parameter θ).

This approach can be problematic since step 2 is not naturally defined on discrete data.

Recently, some articles studied the implementation of the discrete Ridgelet transform. Do and Vetterli proposed in [9] an implementation method of Ridgelet transform based on the use of the finite Radon transform for Z_p^2, the cartesian product of two sets of integers mod p, where p is a prime. This method achieves both invertibility (the inverse transform is stable) and non-redundancy (the associated Ridgelet transform is orthogonal). The obtained denoising results presented in [9] illustrate that this strategy is more effective than the Wavelet transform in recovering straight edges. This transform is not geometrically faithful (the finite Radon transform has an important wrap-around effect) and is only defined for image s such that $s \in l^2_{[0...p-1]\times[0...p-1]}$ where p is a prime number. Moreover this Radon transform integrates over lines that can be rather arbitrarily spread out over the spatial domain and discrete lines in the Fourier domain associated with this decomposition are not closed. This approach is not based on a geometrically faithful notion of Ridgelets and suffers from artifacts (for example in denoising application: figure 10).

In [18], Starck et al. proposed to use an interpolation scheme that substitutes the sampled values of the Fourier transform obtained on the square lattice with sampled values of $\widehat{s}$ on a polar lattice. They use a pseudopolar Fourier domain that offers a notion of polar Fourier domain better adapted to digital data (the digital Fourier domain is viewed as a sequence of squares, not circles). The discrete pseudopolar Fourier transform of a digital image $s \in l^2_{[0...n-1]\times[0...n-1]}$ is defined by sampling the 2-D Fourier transform at the collection of pseudopolar grid points illustrated by figure 2 (from [3]). The paper [18] follows the strategy based on the pseudopolar grid. However, it uses a simple nearest-neighbor interpolation scheme to evaluate pseudopolar grid points in terms of nearby cartesian grid points. More recently Donoho et al. proposed in [3] a fast pseudopolar Fourier transform based on a chirp-Z transform (for the exact evaluation of the 2-D Fourier transform at these non cartesian points). The associated Radon transform (called Slant) is algebrically exact and geometrically faithful. However in order to be invertible this transform requires a fixed factor four of redundancy. Moreover, the inverse transform is ill-conditioned in the presence of noise and requires an iterative approximation algorithm.

In this paper, we propose to use the Fourier strategy for the digital Radon transform. Our lines L_θ are defined with help of the discrete analytical geometry theory in the Fourier domain [2,16]. This solution allows us to have different Ridgelet decompositions according to the arithmetical thickness of

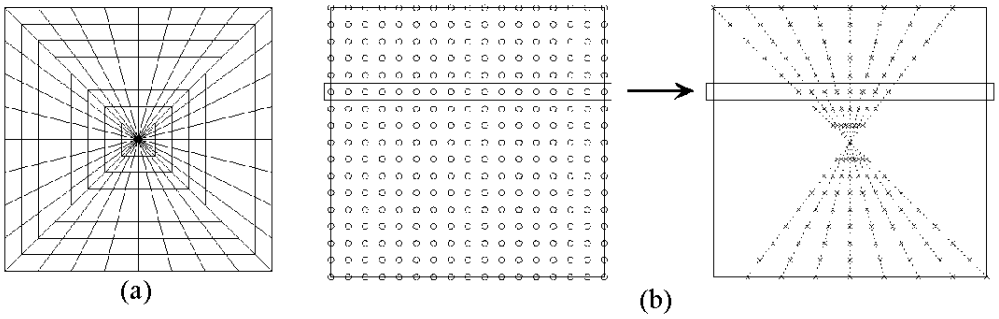

Fig. 2. (a) The pseudopolar grid (b) The conversion from cartesian grid to pseudopolar grid (from [3])

the discrete lines. This approach presents a limited wrap-around effect. As for the Donoho's transform [3], our representation is redundant however the degree of redundancy can be adapted by our thickness parameter. Our Radon backprojection is very simply and permits an exact reconstruction (analytical Radon transform followed by backprojection analytical Radon transform is a one-to-one transform). The objects defined in discrete analytical geometry (3D lines, planes, hyperplanes, ...) allows extensions to 3D and even higher dimensions (see section 4.4).

2.3 Multiscale Ridgelet: Curvelet

The Curvelet transform proposed by Donoho [13] allows us to obtain a multiscale Ridgelet analysis with interscale orthogonality. The Curvelet transform is obtained by filtering and then applying a windowed Ridgelet transform on each bandpass image. The motivation behind the Curvelet transform is that by smooth windowing, segments of smooth curves would look straight in subimages, hence they can be well captured by a local Ridgelet transform. Subband decomposition is used to keep the number of Ridgelets at multiple scales under control by the fact that Ridgelets of a given scale exist in a certain subband. The window's size and subband frequency are linked such that Curvelets have support verifying the key anisotropy scaling relation for curves [13]:

$$width \approx length^2$$

Starck et al. propose a Curvelet transform that uses an undecimated filter bank [18] for the subband decomposition. They applied their digital Curvelet transform to the denoising of some standard images embedded in white noise. These empirical results reported in [18] and based on simple thresholding of the Curvelet coefficients show that this strategy is very competitive with state of the art techniques based on wavelets.

The study of the DART generalization to the Curvelet transform is not the aim of our article but some examples will illustrate how our Ridgelet tranform can be extended to the multiscale approach.

3 Discrete Analytical Ridgelet Transform : DART

The idea behind our associated discrete Radon transform is to represent each direction by a discrete analytical straight line. For this we need a discrete straight line that has a central symmetry and that forms a "good" approximation of the corresponding Euclidean straight line (i.e. direction). Without central symmetry (i.e. if (x, y) and $(-x, -y)$ both belongs to the line), the inverse Fourier transform leeds to imaginery values. This excludes the classical Bresenham discrete 2-D line [4]. Instead we chose discrete analytical 2D lines. It defines not a unique line but a family of lines with a thickness parameter, called arithmetical thickness. The arithmetical thickness provides a control over the transform redundancy factor and properties such as the connectivity of the straight line. This thickness allows us to choose the discrete straight line definition that fits best a given application. The discrete line is analytically defined meaning that the discrete line is defined by equations that allow a precise study of the properties and immediate extensions to higher dimensions. An important body of theory, called discrete analytical geometry, is now available since J-P. Reveillès first proposed such an approach [16].

3.1 Definition and properties of the closed discrete analytical lines

The discrete analytical line we use for our transform are defined as follows [2]:

$$L^{\omega}_{[p,q]} = \left\{ (x_1, x_2) \in \mathbb{Z}^2 \,\middle|\, |qx_1 - px_2| \leq \frac{\omega}{2} \right\}$$

with $[p, q] \in \mathbb{Z}^2$ the direction of the Radon projection (we have $\theta = \arctan\left(\frac{q}{p}\right)$) and ω, a function of (p, q), the arithmetical thickness. J-P. Reveillès introduced the discrete analytical lines in 1991 [16], defined as $0 \leq qx - py + r < \omega$. In this paper, since we need central symmetry, we chose a variant of the closed discrete analytical lines, defined as $0 \leq qx - py \leq \omega$, studied in [2].

It is easy to see that the closed discrete analytical lines $L^{\omega}_{[p,q]}$ have a central symmetry regardless of the value of ω. Moreover, the discrete analytical line can easily be extended to higher dimensions as discrete analytical hyperplanes defined by $|\sum_{i=1}^{n} q_i x_i| \leq \frac{\omega}{2}$ [1].

The arithmetical thickness ω is an important parameter that controls, among other things, the connectivity of the discrete lines: let's consider the closed discrete analytical line $L^{\omega}_{[p,q]}$ and its Euclidean counterpart $\mathcal{L}_{[p,q]} : qx_1 - px_2 = 0$, then:

- For $\omega < \max(|p|, |q|)$, $L^{\omega}_{[p,q]}$ is not connected;
- For $\omega = \max(|p|, |q|)$, $L^{\omega}_{[p,q]}$ is 8-connected. This is called the closed naive line. It is directly related to the distance d_1 since

$$L^{\max(|p|,|q|)}_{[p,q]} = \left\{ M \in \mathbb{Z}^2 \middle| d_1\left(M, \mathcal{L}_{[p,q]}\right) \leq \frac{1}{2} \right\}$$
$$\text{with } d_1(A,B) = \left|x_1^A - x_1^B\right| + \left|x_2^A - x_2^B\right|$$

- For $\omega \geq \max(|p|, |q|)$, $L^{\omega}_{[p,q]}$ is 8-connected.
- For $\omega = \sqrt{p^2+q^2}$, $L^{\omega}_{[p,q]}$ is 8-connected. This is called the Pythagorean line. This type of line is directly related to the distance d_2 since

$$L^{\sqrt{p^2+q^2}}_{[p,q]} = \left\{ M \in \mathbb{Z}^2 \middle| d_2\left(M, \mathcal{L}_{[p,q]}\right) \leq \frac{1}{2} \right\}$$
$$\text{with } d_2(A,B) = \sqrt{\left(x_1^A - x_1^B\right)^2 + \left(x_2^A - x_2^B\right)^2}$$

- For $\omega = |p| + |q|$, $L^{\omega}_{[p,q]}$ is 4-connected. This is called the supercover line and has a theoretical importance [2]. This type of line is directly related to the distance d_∞ since

$$L^{|p|+|q|}_{[p,q]} = \left\{ M \in \mathbb{Z}^2 \middle| d_\infty\left(M, \mathcal{L}_{[p,q]}\right) \leq \frac{1}{2} \right\}$$
$$\text{with } d_\infty(A,B) = \max\left(\left|x_1^A - x_1^B\right|, \left|x_2^A - x_2^B\right|\right)$$

.

- For $\omega \geq |p| + |q|$, $L^{\omega}_{[p,q]}$ is 4-connected.

These results are direct consequence of a well known result in discrete analytical geometry and more recent studies on distances [16,2]. The fact that these lines can be defined with help of distances makes a direct link with mathematical morphology [17].

In this paper we studied the DART with the closed naive lines, the pythagorean lines and the supercover lines.

We use the Fourier domain for the computation of discrete Radon transform: Fourier coefficients of $\widehat{s}$ are extracted along the discrete analytical line $L^{\omega}_{[p,q]}$

$$P^{\omega}_{[p,q]}s = \bigcup_{k\in\mathbb{Z}^+} \widehat{s}(f_1^k, f_2^k) \text{ such that } \left|qf_1^k - pf_2^k\right| \leq \frac{\omega}{2}$$

and we take the 1-D inverse FFT of $P^{\omega}_{[p,q]}s$ on each value of the direction $[p,q]$. Formally, our discrete analytical Radon transform is defined by:

$$R^{\omega}s([p,q],b) = \sum_{k=0}^{K-1} P^{\omega}_{[p,q]}s(k).e^{2\pi j\frac{k}{K}b} \text{ with } K \text{ length of } L^{\omega}_{[p,q]}$$

We must define the set of discrete directions $[p,q]$ in order to provide a complete representation. The set of line segments must cover all the square lattice in the Fourier domain. For this, we define the directions $[p,q]$ according to pairs of symmetric points from the boundary of the 2-D discrete Fourier spectra. Figure 3a illustrates this choice of angles with the covering of the Fourier domain by the associated Euclidean lines. Notice that this set of angles is not equispaced.

Proposition 1 *Let a square lattice be defined as* $\Omega^2_N = [-N;N]\times[-N;N]$. *Let us consider the set of directions* (p_m,q_m) *with* $0 \leq m \leq 2N$, $(p_m,q_m) = (N, m-N)$ *and for* $2N+1 \leq m \leq 4N-1$, $(p_m,q_m) = (3N-m, N)$. *The set of all discrete analytical lines defined by* $|q_m f_1 - p_m f_2| \leq \frac{\omega_m}{2}$ *with* $\omega_m \geq \sup(|p_m|,|q_m|)$ *provides a complete cover of the lattice* Ω^2_N.

The proof of this proposition is obvious since we are dealing here with discrete lines that are at least 8-connected as stated in the previous section. As soon as we take $\omega = \sup(|p_m|,|q_m|) - 1$ the lattice is not covered anymore (because of $L^{\sup(|p_m|,|q_m|)-1=0}_{[0,1]}$ and $L^0_{[1,0]}$). More complex formulas for ω can probably be propose that provide a complete cover and a lower redundancy. This is still an open and somewhat difficult question. In our applications we chose to work only with connected discrete lines.

Figure 3 illustrates the cover of the Fourier lattice (on the first octant) for two different types of discrete lines. The grey value of the pixel represents the redundancy in the projection (number of times a pixel belongs to a discrete line). One isolated line is drawn to illustrate shape of the discrete lines depending on its arithmetical thickness.

- In figure 3b, we show the redundancy for the closed naive lines. They provide a relatively small DART redundancy factor of ≈ 2.05. These lines are well

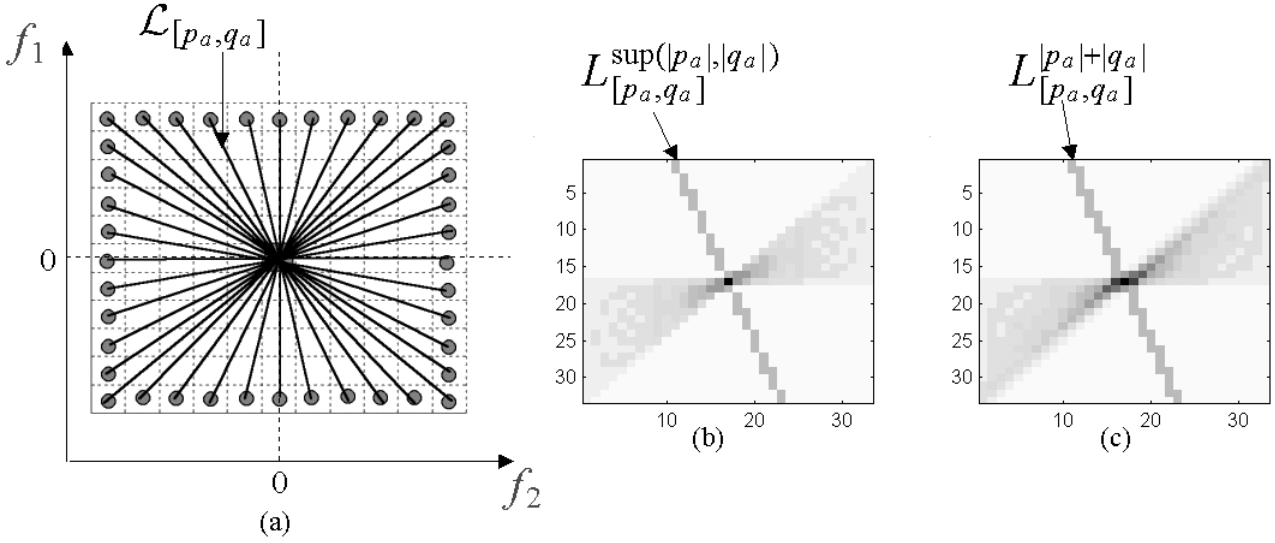

Fig. 3. (a) Cover of the Fourier domain with the Euclidean line $\mathcal{L}_{[p,q]}$. (b) Redundancy on the cover of the Fourier lattice by closed naive lines, (c) by supercover lines

suited for applications such as partial reconstruction where a relatively small redundancy is an asset.

- in Figure 3c, we show the redundancy for the supercover lines. They provide a more important DART redundancy factor of ≈ 3.05. These lines are well suited for applications such as denoising.
- The pythagorean lines provide an intermediate DART redundancy factor of ≈ 2.35.

We now give two examples of the discrete analytical Radon transform in action. We propose a comparison with the differents solutions proposed in the literature. The papers of Stanford [18] reference a Matlab Toolbox developed by Stanford researchers for performing Ridgelet and Curvelet analysis. Although this code is actually not open to the public. In place, we use the Radon transform developped by Mathworks that is based on a geometrically faithful notion of Radon and that does not presents wrap-around effect. The result of the Mathworks transform is visually similar than the Stanford transform. The code of Do and Vetterli [9] is open to the public (http://lcavwww.epfl.ch/~minhdo). In figure 4, we show the result of the discrete Radon decomposition of an array containing a single nonzero entry. We observe that :

- In this case, the Radon transform follows a broken line as for the Mathwork transform.
- The finite Radon transform of Do and Vetterli has an important wrap-around effect and is difficult to interpret.

- Our transform obtains a broken line without wrap-around effect.

Figure 4d illustrates the influence of the increasing of the redundancy of the decomposition (in this case, supercover lines are used) : the Radon is an interpolated broken line.

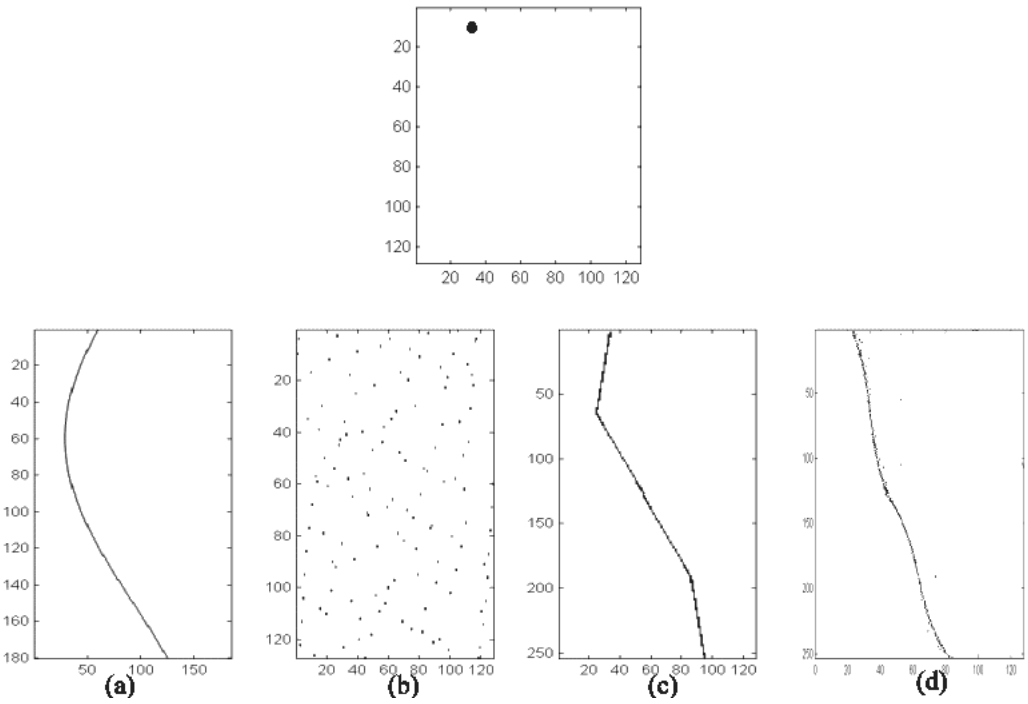

Fig. 4. The Radon transform of a point : (a) with a geometrical strategy (b) with the Do and Vetterli approach. (c) with our strategy using the closed naïve lines, (d) the supercover lines

We want now to find for a given coefficient $([p,q],b)$ of the Radon transform, which pixels have contributed [3]. For this, we apply the Radon backprojection. Our analytical reconstruction procedure works as follows:

(1) Compute the 1-D FFT transform for each set $R^{\omega}s([p,q],.)$
(2) Substitue the sampled value of $\widehat{s}$ on the lattice where the points fall on lines $L^{\omega}_{[p,q]}$ with the sampled value of $\widehat{s}$ on the square lattice.
(3) Apply the 2-D IFFT transform.

The previous procedure allows us to obtain an exact reconstruction if the set of directions of lines provide a complete cover of the square lattice. To make a comparison, we use the IRadon procedure of Mathworks that uses the filtered backprojection algorithm (based on an interpolation in the Fourier domain) to perform the inverse Radon transform. Notice that the results obtained with this backprojection are visually similar to Stanford's results. We use also the code of Do and Vetterli. All these backprojections are presented in figure 5.

We can see that our strategy does not exhibit geometrical distortions and a very limited wrap-around artifacts (that could be removed by zero-padding in the Fourier domain). The results are similar for the different types discrete analytical lines.

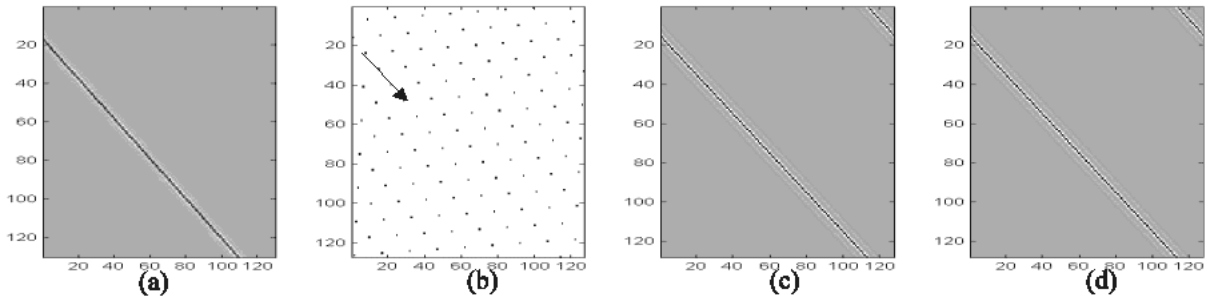

Fig. 5. The Radon backtransform of a point : (a) with a geometrical strategy (b) with the Do and Vetterli approach. (c) with our strategy using the closed naive lines, (d) and the supercover lines

3.3 Definition of the DART

Now, to obtain the Ridgelet transform, we must take a 1-D wavelet transform along the radial variable in Radon space. The choice of discrete one-dimensional wavelet transform is discussed by Starck et al. in [18]. They indicate that experience has shown that compactly-supported wavelets can lead to many visual artifacts when used with nonlinear processing. This is due to the lack of localization of such compactly-supported wavelets in the frequency domain. The first Stanford implementations have made the choice of bandlimited wavelets, whose support is compact in the Fourier domain. For this, they use the periodic discrete Meyer wavelet that consists of a system of division in the frequential domain. The discrete Meyer wavelet transform is studied in Kolaczyk's thesis [14]. After that, Starck et al. chose a specific overcomplete system: they define the scaling function in the frequency domain as a renormalized B_3-spline and the wavelet function as the difference between two consecutive resolutions. With this choice, each subband is sampled above the Nyquist rate, hence avoiding aliasing (this phenomenon is present when a nonlinear processing is applied on orthogonal wavelet transforms). Do and Vetterli use classical decimated Symlet Wavelet for the denoising problematic.

In this article, we do not propose a "definitive" solution associated with the different discrete analytical lines. The choice of the type of 1-D wavelet transform depends of the goal of the transform. This wavelet transform can be decimated or undecimated and the wavelet base can be adapted according to the application, as for the classical wavelet decomposition. In the following sec-

tion, we compare the use of Meyer wavelets (whose support is compact in the Fourier domain) and the use of decimated/undecimated compactly-supported wavelets for two applications : denoising and partial reconstruction.

4 Illustration of the DART

4.1 naive lines vs pythagorean lines vs supercover lines

A. Denoising

The denoising procedure by Ridgelet transform consists simply in thresholding the Ridgelet coefficients and computing the inverse Ridgelet transform. The thresholding is performed with help of an undecimated method developed for the wavelet decomposition [8,7]. The redundancy of the wavelet decomposition, associated with this method, reduces artifacts that appear after thresholding. Let r_s^ω be the noisy undecimated Ridgelet coefficients, we use the following hard-thresholding:

$$r_s^\omega([p,q],a,b) = \begin{cases} r_s^\omega([p,q],a,b) \text{ if } r_s^\omega([p,q],a,b) \geq \alpha\sigma \\ 0 \text{ otherwise} \end{cases}$$

α can be defined as $\alpha = \sqrt{2\log(N)}$ [10]. We can use two strategies for the estimation of the variance of the noisy Ridgelet coefficients σ:

- We consider that the DART is not norm-preserving and the variance depends thus on the projection index. In this case, the individual variance is estimated using the absolute median of the wavelet decomposition's first scale of each radial projection (if the wavelet decomposition is norm-preserving).
- By evaluating the DART (defined with Daubechies D20 wavelets) of a few standard white noise images, we have observed that the variance of noisy coefficients remains constant. The variance can then be estimated before the Ridgelet transform and used for all the Ridgelet transform.

Our experiments have shown that the first strategy is better for denoising with the DART (the SNR measure of reconstructed image is higher). We use thus this first method.

In order to illustrate precisely the result of the denoising algorithm with different types of discrete analytical lines we have generated an artificial image

(Figure 6a) and added important white noise (Figure 6b). The SNR [1] of the noisy image is equal to 15 dB. Figures 6c, d and e are the results obtained with the three definitions of discrete analytical lines (naive, pythagorean and supercover) and with the Daubechies D20 wavelets. For a more redundant decomposition (based on supercover discrete lines, figure 6e) the denoising result is better than for a less redundant decomposition (figure 6c): the edge is reconstructed more precisely and the uniform areas are smoother. As for the wavelet decomposition, overcompletness provides advantages for denoising.

For comparison the result of a denoising carried out by classical decimated wavelet coefficient threshold (figure 6f) is also given. The result is obtained with a decimated decomposition by Daubechies D20 wavelets and a "hard" thresholding. The threshold is based on the noise variance, as Donoho *et al.* introduced in [10]. Noise variance is estimated using the absolute median of the first decomposition scale. The wavelet method obtains the best SNR measure, but it exhibits numerous blemishes, that are a result of the nonlinear processing with critical sampling. This experiment illustrates the limits of the SNR measure since it does not quantify well this type of artifacts.

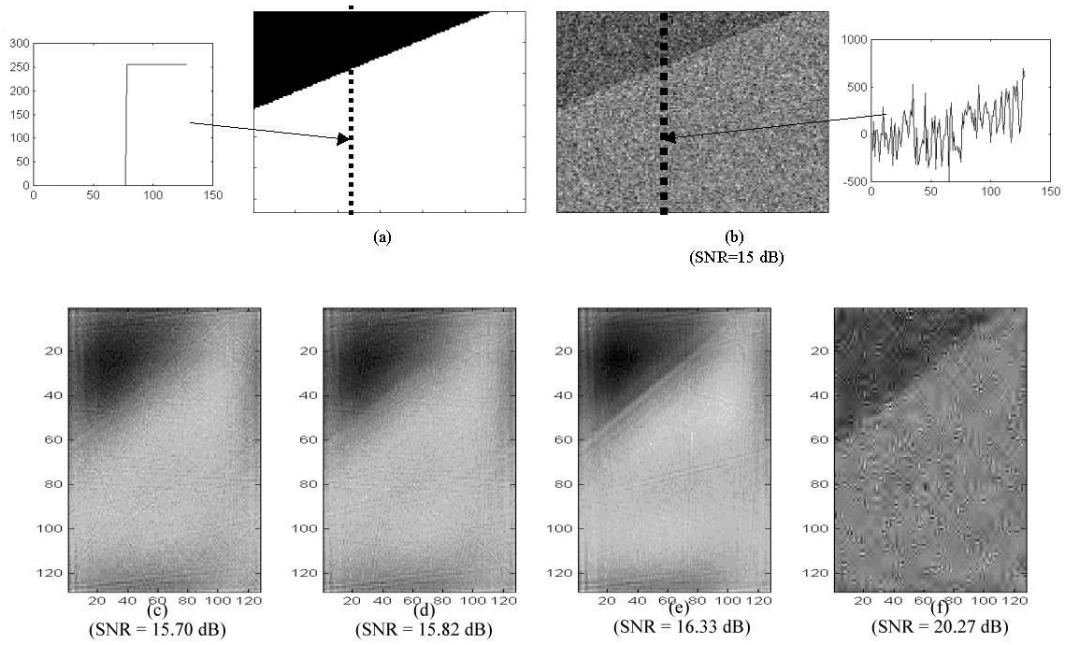

Fig. 6. (a) original image (b) noisy image (to show more precisely the effect of the noise we plot a vertical line of each image). (c) denoising with naive lines (d) denoising with pythagoricean lines (e) denoising with supercover lines (f) denoising with decimated wavelet transform

B. Partial reconstruction

[1] All the SNR measures are done with the Stanford Matlab function.

Contrary to the denoising problematic, for a partial reconstruction, redundancy is of course not interesting. Figure 7 compares partial reconstruction of an artificial image by using the 30% largest naive-DART coefficients with reconstruction by using the 30% largest supercover-DART coefficients. This illustrates how the arithmetical thickness of the discrete lines employed in our Ridgelet transform influences the quality of the "compressed" image. The lower redundancy representation (naive discrete lines) preserves all the features of the original image after a simple thresholding (Figure 7 b). On the other hand, with the higher redundancy representation (supercover lines) we loose features and the image is globally of lower quality.

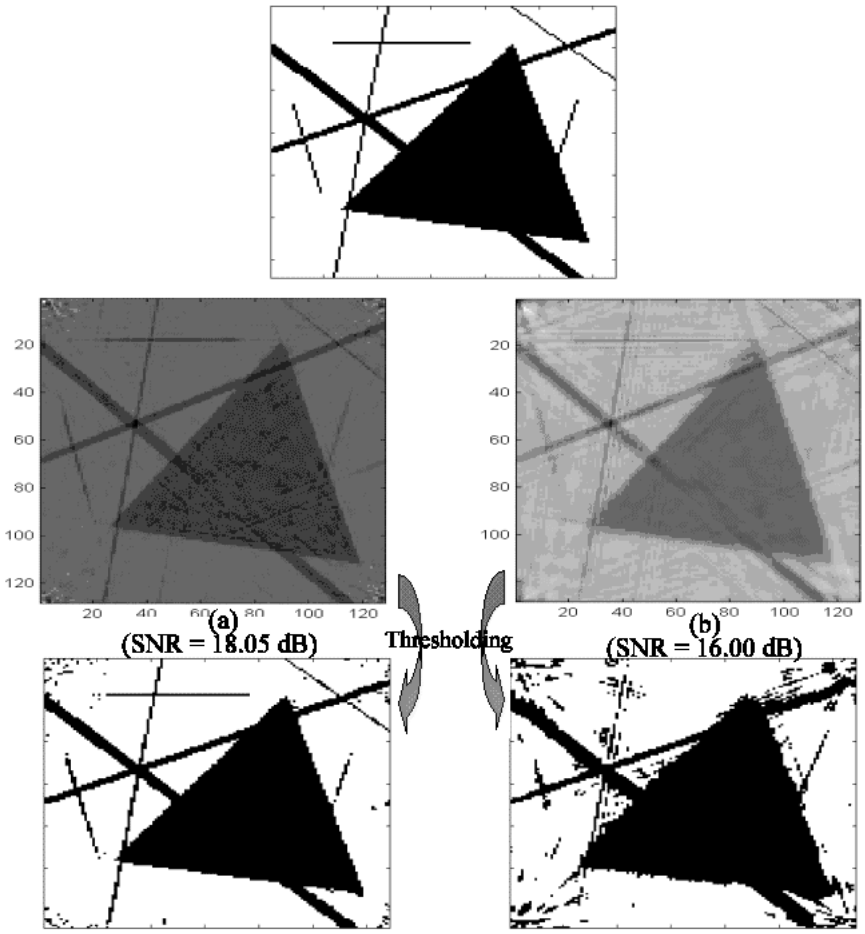

Fig. 7. Partial reconstruction of an artificial image (a) naive-DART (b) supercover-DART

We discuss now the choice of 1-D wavelet transform with the DART. For this, several 1-D wavelet transforms were tested along the radial variable in discrete analytical Radon space (for these experiments, we use only the naive discrete line definition, the results are equivalent with the others types of lines):

(1) The discrete Meyer wavelet (whose support is compact in the Fourier domain) transform.
(2) The Daubechies D20 wavelet (whose support is compact in the time domain) transform.
(3) The undecimated Daubechies D20 wavelet transform.
(4) The overcomplete system based on the work of Starck et al. [18] (whose support is compact in the Fourier domain).

A. Denoising

Figure 8 considers an object used by Do and Vetterli in their paper [9], and compares the denoising of this image by thresholding of the DART with different wavelet bases. We use the SNR and the visual analysis to measure the performance. We observe that :

- The undecimated methods offer superior performances over orthogonal wavelet decompositions.
- With decimated wavelet decomposition, the compactly-supported wavelets in the frequency domain obtain better SNR measures than compactly-supported wavelets in the time domain.
- The Starck-DART reconstruction and undecimated Daubechies D20 DART reconstruction are very similar.

For denoising with the DART, we can not conclude that the undecimated compactly-supported wavelets in the frequency domain enjoys superior performance over the undecimated compactly-supported wavelets in the time domain. However, in this study, we use time filters (D20 filters) that have very large supports. In this case the filter profile in Fourier domain converges rapidly to 0 after the cut-off frequency. If the same experiments are done with too small filters, the reconstructed image will contain some disturbing artifacts.

More generally, we have generated a set of noisy images from both Do's Object image and Lenna image. We have then compared the four different filtering procedures. These experimental results have confirmed that the Starck-DART reconstruction and undecimated Daubechies D20 DART reconstruction are similar and seem to be the better choice.

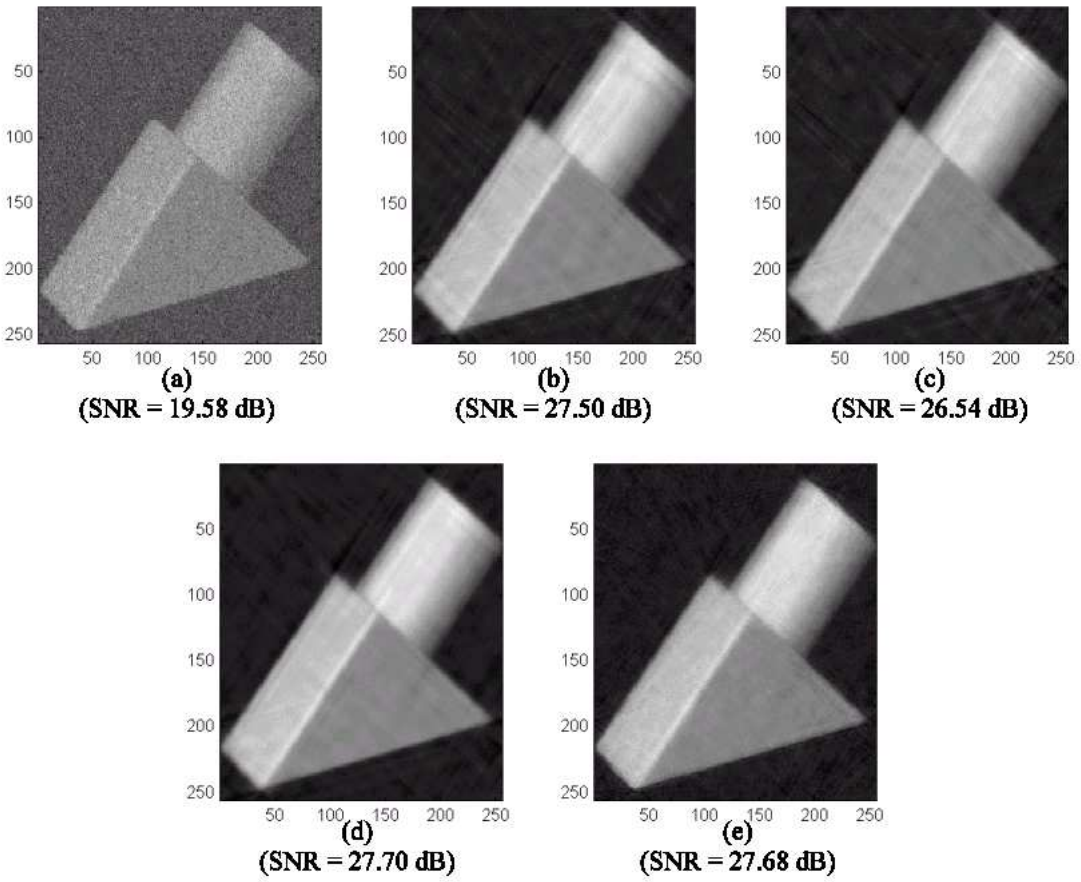

Fig. 8. (a) Noisy image (b) denoising with the Meyer-DART transform (c) denoising with D20-DART transform (d) denoising with undecimated D20-DART transform (e) denoising with Starck-DART transform

B. Partial reconstruction

We now consider the partial reconstruction of Do's object by the 30% largest DART coefficients (figure 9). Only the decimated wavelet transforms are tested since the redundancy is irrelevant for partial reconstruction. We observe that, in the frequency domain, the more compact the wavelet support is, the better the SNR measure is. These results confirm Stanford's experience. However, comparing the different reconstructed images, one can hardly see the difference. We have generated a set of partial reconstructions from both Do's object and Lenna. These experiments confirm previous visual analyzes: partial reconstructions from D20-DART and Meyer-DART are equivalent.

From these experiments (denoising and partial reconstruction), we propose to use the D20 wavelets for the DART because the D20 basis can be simply associated to an orthogonal transform or an undecimated transform (with the "à trous" algorithm) and moreover this base is norm-preserving.

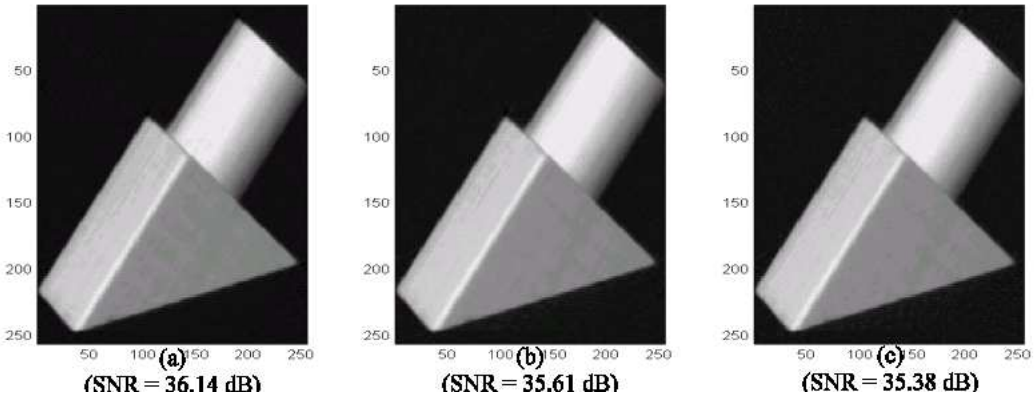

Fig. 9. Partial reconstruction of Do's image (a) Meyer-DART (b) D20-DART (c) D8-DART

4.3 DART vs litterature Ridgelet transform

We briefly compare the DART with the other Ridgelet transform implementations we know about. As we have said the Stanford's code is actually not open to the public (a comparison with Stanford's results in PSNR terms is done in the following section). In place, we use the Radon transform developped by Mathworks that satisfies a geometrically faithful notion of Radon (with no wrap-around effect). This allows us to measure the importance of having or not a wrap-around effect.

A. Denoising with DART and Local DART

Figure 10 compares the denoising of the very noisy Do's image (SNR 18.73 dB) by thresholding the Ridgelet transform:

- The Ridgelet based on "geometrical" Radon transform (Mathworks code) and the Starck overcomplete wavelet system. In this case, the noise variance is estimated by evaluating the "geometrical" Ridgelet transform of standard white noise images (as proposed in [18]).
- The Do and Vetterli orthogonal Ridgelet.
- The DART based on supercover lines and undecimated D20 wavelets.

We illustrate also the results obtain with decimated and undecimated wavelet transform (implemented by Stanford in the toolbox Wavelab).

We observe that :

- The "geometrical" Ridgelet and the DART reconstruction does not contain the many blemishes that one sees in the wavelet reconstructions. The SNR measures of these two transforms are better.

- The decimated wavelet transform displays disturbing artifacts. The use of a redundant wavelet transform considerably reduces the number of artifacts.
- The Do's Ridgelet transform corresponds to a critical sampling. The reconstruction associated with a nonlinear processing contains thus many visual artifacts.
- The DART enjoys superior performance over Geometrical Ridgelet transform [2].

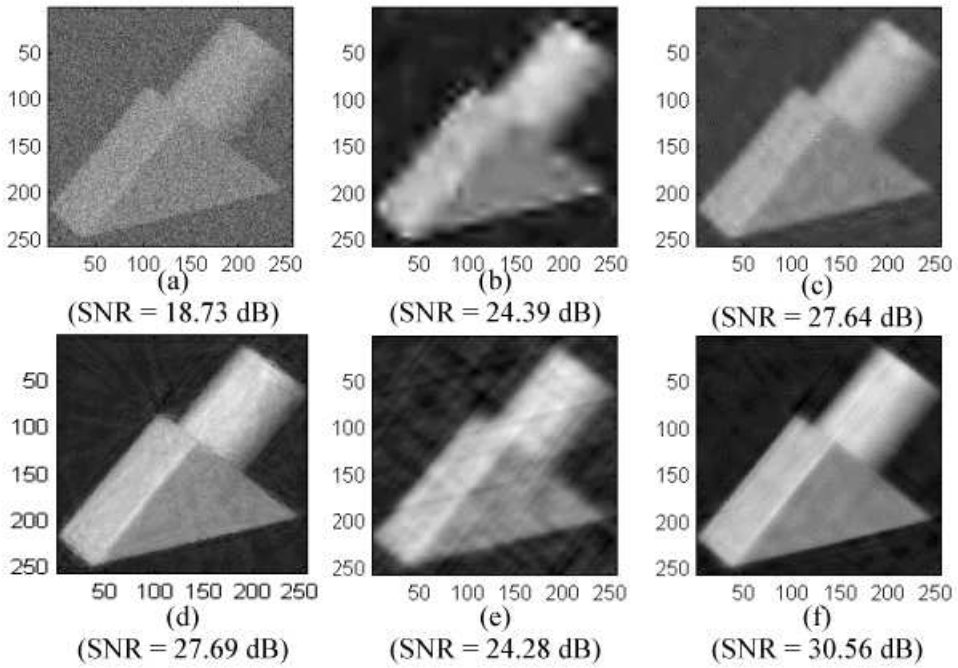

Fig. 10. (a) noisy image ; denoising with (b) the decimated wavelet transform (c) the undecimated wavelet transform (d) the undecimated geometrical Ridgelet (e) the Do and Vetterli approach (f) The supercover-DART

B. Extension to Local DART and Curvelet DART

The DART can be easily extended to a local transform by a smooth partitioning, or more generally to a Curvelet transform by the following steps:

- Decompose the image into a set of wavelet bands.
- Each subband is smoothly windowed into squares.
- Analyse each square by the DART.

Notice that the subbands used in the discrete Curvelet transform of continuum

[2] We can obtain better results with the "Mathworks" Radon transform by using an other level of threshold. However, because the Radon and the Wavelet transform associated with this strategy is not norm-preserving, it is difficult to define a general level of threshold.

functions have the non-standard form $\left[2^{2l}, 2^{2l+2}\right]$. Starck et al. propose to use a specific overcomplete subband filtering: the wavelet function is defined as the spatial difference between two consecutive resolutions. We extend our digital Ridglelet transform with the same principle, but we substitute the Starck's overcomplete subband filtering with an undecimated quincunux wavelet decomposition in order to preserve the interscale orthogonality. Moreover this wavelet transform preserves the variance of the noise. The comparison between Ridgelet denoising results and Curvelet denoising results is however not the subject of this paper. These experiments are done precisely by Starck et al. (http://www-stat.stanford.edu/~jstarck). We illustrate only how the DART can be extended to the Curvelet formalism.

To illustrate the local DART and the new discrete Curvelet transform based on discrete analytical lines, we have developed an example of denoising algorithm. As for the Ridgelet transform, the denoising by Curvelet transform consists simply in thresholding the Curvelet coefficients and computing the inverse Curvelet transform. For the estimation of the variance σ of the noisy Curvelet-DART coefficients, we consider that the Curvelet-DART is "norm preserving". The noise variance is then estimated before the Curvelet transform.

In our example, a Gaussian noise with a standard deviation equal to 60 was added to the classical Lenna image (Figure 11a). Several methods were used to filter the noisy image: thresholding of the undecimated wavelet transform (Figure 11b), thresholding of "supercover" DART (Figure 11c), thresholding of local "supercover" DART (Figure 11d), thresholding of Curvelet DART based on supercover discrete lines and undecimated quincunux scheme (Figure 11e). We observe that the Curvelet DART and Local DART enjoy superior performance over the other transforms. For these decompositions the analysis is better localized in the spatial domain. This property eliminates the parasitic lines present in the DART reconstruction and due to the selection of an important contour in an area of the image. As for the Ridgelet transform, we can use other definitions of discrete analytical lines for Local DART and Curvelet DART.

To study the dependency of these methods on the noise level, we generated a set of noisy images from both Do's Object and Lenna. We then compared the different filtering procedures. This series of experiments is summarized in Figure 12 for Lenna. These experimental results show that the Local DART and Curvelet-DART correspond, in general, to the better results.

In order to make a comparison with Stanford's results, we use one of the example of denoising proposed in [18]: a Gaussian noise with a standard deviation equal to 20 is added to the Lenna image (size: 512 by 512). The reconstruction by local DART and Curvelet-DART are presented figure 13. The results of Stanford's algorithm are visible at the website http://www-

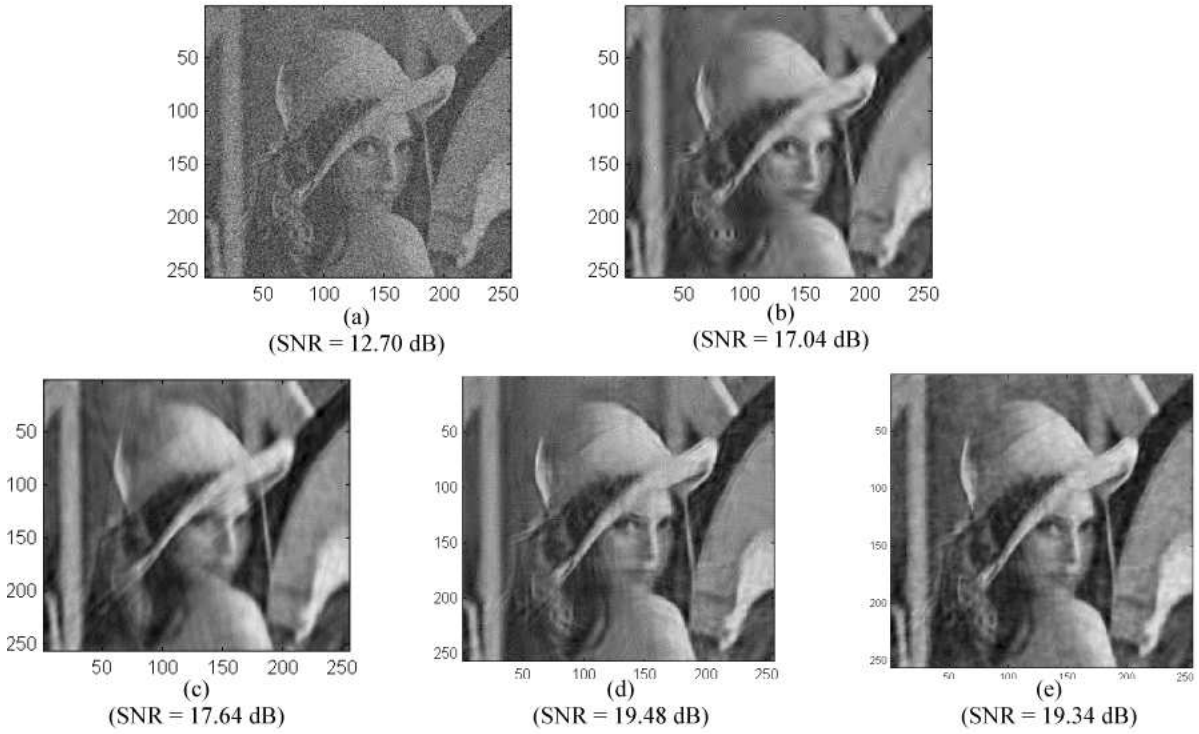

Fig. 11. (a) noisy image (b) denoising with the undecimated wavelet transform (c) denoising with DART based on supercover lines (d) denoising with local DART based on supercover lines (e) denoising with DART-Curvelet based on undecimated quinconx wavelet transform and supercover lines

	64 (1)	32 (1)	16 (1)	Curvelet
DART	31.42	31.38	30.61	31.23
Stanford	30.79	30.97	30.87	31.95

Table 1
PSNR measures of DART and Stanford reconstructions. (1) Size of the window

stat.stanford.edu/~jstarck. From the figure 13 and the Stanford Web site, one can not see important differences between the Stanford strategy and the DART strategy.

In order to make an quantitative measure we used the PSNR. We indicate in the table 1,

- The PSNR values [3] after filtering with the local DART and Curvelet-DART.
- The PSNR values after filtering with the Stanford algorithm indicated in [18].

[3] The PSNR measures of DART are done with the Stanford Matlab function.

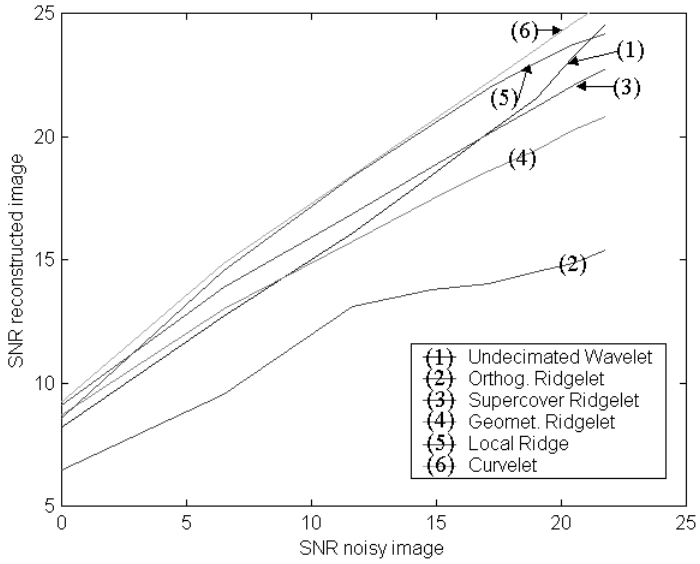

Fig. 12. SNR of reconstructed image versus SNR of noisy image for different representation. The panel corresponds to Lenna.

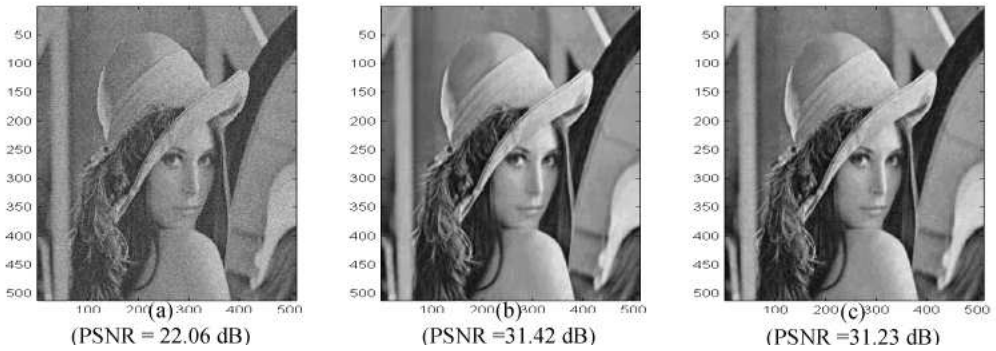

Fig. 13. (a) noisy image with the same level of noise than [18] (b) denoising with local DART based on supercover lines (c) denoising with DART-Curvelet based on undecimated quincunux wavelet transform and supercover lines.

These measures confirm the visualy analysis: the Stanford reconstruction and DART reconstruction are very similar. However, as we have said, the back-projection DART algorithm is simpler and the DART representation is more flexible (with the variable line thickness).

Notice that Color denoising results obtained with the DART are presented in [6].

C. Partial reconstruction

We now consider the partial reconstruction of Do's object by the 512 most

important Ridgelet coefficients (figure 14). Only the decimated wavelet transforms associated with naive lines are tested. Since our decomposition is redundant, we observe that the DART is not adapted to this problematic contrary to the orthogonal wavelet representation and Do's Ridgelet. However in order to obtain a more sparse representation, we use the strategy called ortho-Ridgelet by Stanford and introduced very recently in [11]. This transform may be viewed as a discrete Radon transform followed by an orthogonal 2-D wavelet transform (we obtain ortho-Ridgelets by taking the wavelet transform along the angular variable of the Ridgelet projection). The ortho-Ridgelet representation is more sparse: the transform along the angular variable has compressed the laterally features of the Ridgelet transform into point-like features. If we apply this $\theta-$wavelet transform to the DART representation, we obtain for the partial reconstruction a result that is close to Do's result. However the ortho-DART reconstruction has a smaller SNR measure than the two orthogonal transforms. This result is a first experimentation and needs to be developed (choice of the best basis along the angular variable, a local approach ...).

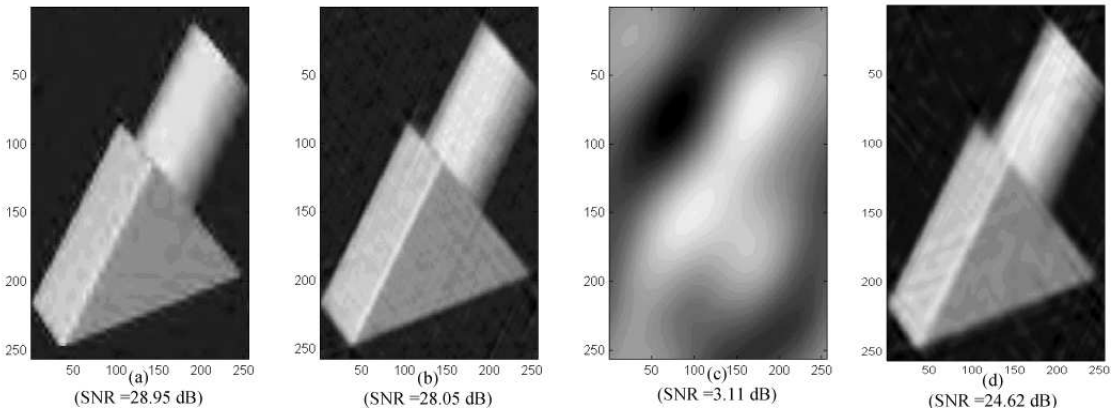

Fig. 14. Partial reconstruction of Do's image (512 coefficients) (a) Wavelet (b) Do's Ridgelet (c) Naive DART. Bad result because of the redundancy (d) Naïve ortho-DART

4.4 DART 3-D ?

As for the 2-D domain, the 3-D Radon transform of an object is related to its 3-D Fourier transform via the central slice theorem: the 3-D Radon transform can be obtained by applying the 1-D inverse Fourier transform to the 3-D Fourier transform restricted to radial lines going through the origin. Once again, we propose to extract the Fourier coefficients along a 3-D discrete analytical line going through the origin. Once a discrete 3-D line is defined, the principle of the method is the same as in the 2-D case with the same properties (exact reconstruction, rapidity, flexible definition). This idea works well for the

supercover model as the 3-D supercover discrete analytical line is connected (see example in figure 15). Thus the set of 3-D supercover lines covers the 3-D Fourier cubic lattice if we define the line directions according to pairs of symetric border points of the lattice. The definition of a 3-D supercover line of direction $[p, q, r]$ is given by [2]:

$$|qx_1 - px_2| \leq \frac{|p| + |q|}{2}$$
$$|rx_1 - px_3| \leq \frac{|p| + |r|}{2}$$
$$|rx_2 - qx_3| \leq \frac{|q| + |r|}{2}$$

In the same way, all the supercover of all m-flats in dimension n are well defined [2]. This allows us to generalize this approach to 3-D planes (see example in figure 15) and dimension n. For the other models (naive and pythagorean for example) however the definition and the extension to 3-D lines or higher dimensions is more problematic. For instance, the 3-D naive discrete analytical line is not connected in general and does not ensure a complete cover of the 3-D cubic Fourier lattice. We hope to report on this developpements in a forthcoming paper.

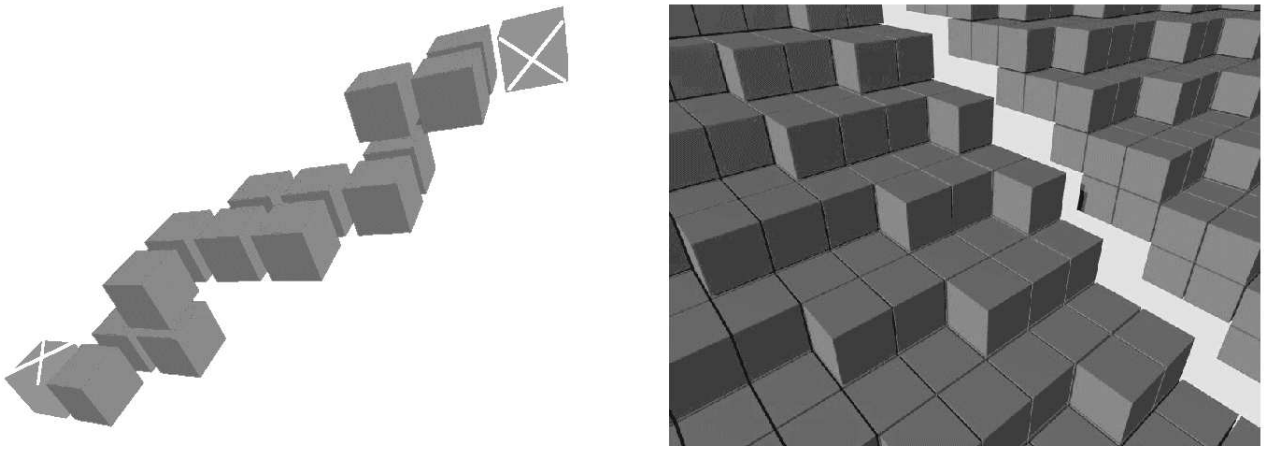

Fig. 15. Discrete analytical 3-D line and plane

5 Conclusion

In this paper, we have proposed a new strategy for implementing the discrete Ridgelet transform. So far, the developement of the discrete Ridgelet transform has been investigated by two teams (Stanford and EPFL) in previous

works. Our innovative choice is to use the formalism of the discrete analytical geometry theory in the Fourier domain, in order to define a new discrete Ridgelet transform: the Discrete Analytical Ridgelet Transform (DART).

The DART algorithm is easy to implement. It provides an exact reconstruction property: the DART followed by a reverse DART is a one-to-one transform. Our experiments have shown that our approach presents a limited wrap-around effect, that does not influence the denoising or partial reconstruction results. Moreover, by using the analytical formalisation, we define a flexible Ridgelet transform: we can define different DART decompositions according to the arithmetical thickness of the analytical discrete lines. As for Stanfords transform, our representation is redundant but the transform redundancy factor depends on the type of the discrete lines used and can be adapted for each application.

Our DART uses a 1-D wavelet transform based on Daubechies D20 wavelet. Our experiments have shown that this basis associated with the analytical Radon transform obtains satisfactory results for the two studied problematics. Moreover, this basis can be simply associated to an orthogonal transform for partial reconstruction or to an undecimated transform for denoising, and it is norm-preserving. We have seen that if, instead, we use a basis that is compactly supported in the Fourier domain (orthogonal or redundant), it does not improve the results of the DART, but the decomposition is less flexible.

We have illustrated the performances of the DART for denoising problematics, even with very noisy images (with gaussian noise). This study indicates that the Local-DART and the Curvelet-DART thresholding rivals Stanford's Ridgelet denoising results, that are considered as the reference for Ridgelet's denoising applications, and more generally, classical denoising techniques that have been developped over the last decade. Howerver, contrary to the Stanford strategy, the reverse DART does not require an iterative approximation algorithm and the redundancy factor of the representation is not fixed.

This work can be extended in several directions. One of the theoretical questions in discrete geometry is the problem of defining an arithmetical thickness function that provides a smaller redundancy and a cover of the Fourier lattice. This is still an open and difficult arithmetical problem. One of the most important interests of the discrete analytical approach is the possibility to extend easily our work to 3-D. We are currently investigating the application of a 3-D DART to the denoising process of animated video images. In this paper we present some first thoughts abouth these questions.

We are also considering extending our "partial reconstruction" algorithm with more sophisticated representations. The ortho-Ridgelet proposed by Stanford seems to obtain good results for partial reconstruction [12] and constitutes an

interesting new area of research.

References

[1] E. Andres, R. Acharya, and C. Sibata. Discrete analytical hyperplanes. *Graphical Models and Image Processing*, 59(5):302–309, 1997.

[2] Eric Andres. Modélisation analytique discrète d'objets géométriques. Habilitation, Université de Poitiers, 2000.

[3] A. Averbuch, R. Coifman, D. Donoho, and M. Walden. Fast slant stack: a notion of radon transform for data in a cartesian grid which is rapidly computible, algebraically exact, geometrically faithful and invertible. Technical report, Stanford University, 2000.

[4] J. Bresenham. Algorithms for computer control of a digital plotter. *IBM Sys. Journal*, 4(1):25–30, January 1965.

[5] E. Candès. *Ridgelets: Theory and Applications*. PhD thesis, Stanford, 1998.

[6] P. Carré and E. Andrès. Ridgelet transform based on reveillès discrete lines. In *DGCI'02*. (Published in Lecture notes in Computer) Springer-Verlag, April 2002. Bordeaux, France.

[7] P. Carré, H. Leman, C. Marque, and C. Fernandez. Denoising the EHG signal with an undecimated wavelet transform. *IEEE Trans. on Biomedical Engineering*, 45(8):1104–1113, September 1998.

[8] R. Coifman and S. Donoho. Translation-invariant de-noising. In A. Antoniadis and G. Oppenheim, editors, *Wavelets and Statistics*, volume 103 of *Lecture Notes in Statistics*, pages 125–150, New York, 1995. Springer-Verlag.

[9] M. Do and M. Vetterli. Discrete ridgelet transforms for image representation. Submitted to IEEE Trans. on Image Processing, April 2001.

[10] D. Donoho. Wavelet shrinkage and w.v.d.: A 10-minute tour. Technical report, Standford University, 1992.

[11] D. Donoho. Orthonormal ridgelets and linear singularities. *SIAM Journal on Mathematical Analysis*, 31(5):1062–1099, 2000.

[12] D. Donoho and A. Flesia. Digital ridgelet transform based on true ridge functions. Technical report, Stanford University, January 2002.

[13] D. L. Donoho and Emmanuel J. Candès. Curvelets: A surprisingly effective nonadaptive representation of objects with edges. Technical report, Stanford University, 1999.

[14] E. Kolaczyk. *Wavelet Methods for the Inversion of Certain Homogeneous Linear Operators in the Presence of Noisy Data*. PhD thesis, Stanford University, October 1994.

[15] S. Mallat. A theory for multiresolution signal decomposition: the wavelet transform. *IEEE Trans. on PAMI*, 11(7):674–693, 1989.

[16] Jean-Pierre Reveillès. Géométrie discrète, calcul en nombres entiers et algorithmique. Habilitation, Université Louis Pasteur de Strasbourg, 1991.

[17] J. Serra. *Image Analysis and Mathematical Morphology.* Acamedic Press, London, 1992.

[18] J. L. Starck, E. J. Candès, and D. L. Donoho. The curvelet transform for image denoising. Technical report, Department of Statistics, Stanford, November 2000.